

MAGNETIC SENSITIVITY IN THE WING SCATTERING POLARIZATION SIGNALS OF THE HYDROGEN LYMAN- α LINE OF THE SOLAR DISK RADIATION

E. ALSINA BALLESTER¹, L. BELLUZZI^{1,2}, AND J. TRUJILLO BUENO^{3,4,5}

Draft version August 14, 2019

ABSTRACT

The linear polarization produced by scattering processes in the hydrogen Ly α line of the solar disk radiation is a key observable for probing the chromosphere-corona transition region (TR) and the underlying chromospheric plasma. While the line-center signal encodes information on the magnetic field and the three-dimensional structure of the TR, the sizable scattering polarization signals that the joint action of partial frequency redistribution and J -state interference produce in the Ly α wings have generally been thought to be sensitive only to the thermal structure of the solar atmosphere. Here we show that the wings of the Q/I and U/I scattering polarization profiles of this line are actually sensitive to the presence of chromospheric magnetic fields, with strengths similar to those that produce the Hanle effect in the line core (i.e., between 5 and 100 gauss, approximately). In spite of the fact that the Zeeman splitting induced by such weak fields is very small compared to the total width of the line, the magneto-optical effects that couple the transfer equations for Stokes Q and U are actually able to produce sizable changes in the Q/I and U/I wings. We find that magnetic fields with longitudinal components larger than 100 G produce an almost complete depolarization of the wings of the Ly α Q/I profiles within a ± 5 Å spectral range around line center, while stronger fields are required for the U/I wing signals to be depolarized to a similar extent. The theoretical results presented here further expand the diagnostic content of the unprecedented spectropolarimetric observations provided by the Chromospheric Lyman-Alpha Spectropolarimeter (CLASP).

Subject headings: line: profiles — polarization — scattering — radiative transfer — Sun: chromosphere — Sun: transition region

1. INTRODUCTION

The linear polarization produced by scattering processes in ultraviolet (UV) resonance lines of the solar disk radiation encodes key information on the plasma of the upper solar chromosphere and transition region (TR). For example, it is known that the line-center scattering polarization signals are sensitive to magnetic fields via the Hanle effect (e.g., Landi Degl'Innocenti & Landolfi 2004, hereafter LL04). Of particular interest is the hydrogen Ly α resonance line at 121.6 nm, the strongest emission line in the solar UV spectrum. A few years ago, the Chromospheric Lyman-Alpha Spectropolarimeter (CLASP) sounding rocket experiment, motivated by theoretical predictions based on radiative transfer (RT) calculations (Trujillo Bueno et al. 2011; Belluzzi et al. 2012; Štěpán et al. 2015), discovered conspicuous scattering polarization signals in Ly α (see Kano et al. 2017). Theoretical modeling of the observed Stokes Q/I and U/I line-center signals recently allowed us to constrain the magnetic field strength and geometrical complexity of the corrugated surface that delineates the chromosphere-corona TR (Trujillo Bueno et al. 2018).

While the line-center photons of the hydrogen Ly α line stem mainly from the TR, the wing photons encode information on the underlying chromospheric layers (e.g., at $\Delta\lambda = \pm 1$

Å from the line center, the height in the solar atmosphere where the optical depth is unity lies a few hundred kilometers below the TR). Unlike the Q/I and U/I line-center signals, which are sensitive to the presence of magnetic fields in the TR via the Hanle effect, the wing signals have always been thought to be sensitive only to the thermal structure of the solar atmosphere (e.g., Belluzzi et al. 2012). The main aim of the present paper is to show that the wings of the Q/I and U/I profiles of the hydrogen Ly α line are sensitive to the presence of magnetic fields in the solar chromosphere, with strengths similar to those that characterize the onset of the Hanle effect in the line core. The physical mechanism at the origin of this magnetic sensitivity is as follows.

In some resonance lines for which the effects of partial frequency redistribution (PRD) produce large Q/I wing signals, the $\rho_V U$ and $\rho_V Q$ magneto-optical (MO) terms of the transfer equations for Stokes Q and U , respectively, can induce a significant magnetic sensitivity in the line's scattering polarization wings. Given that in the line wings ρ_V is significant already for relatively weak magnetic fields, the above-mentioned $\rho_V Q$ term introduces sizable, magnetically sensitive, U/I wing signals. In turn, such large U/I wing signals allow the $\rho_V U$ term to introduce a magnetic sensitivity in the Q/I wing signals. This mechanism causes both a rotation of the plane of linear polarization as the radiation travels through the solar atmosphere (see Alsina Ballester et al. 2017) and an effective decrease of the degree of total linear polarization (see Alsina Ballester et al. 2018). Recent RT investigations have indicated that such MO effects should play an important role in the wings of many strong chromospheric lines, such as the Mg II k line (Alsina Ballester et al. 2016), the Mg II h & k lines (del Pino Alemán et al. 2016), the Sr II 407.8 nm line (Alsina Ballester et al. 2017), and the Ca I 422.7 nm line

ernest@irsol.ch

¹ Istituto Ricerche Solari Locarno, CH-6605 Locarno Monti, Switzerland

² Kiepenheuer-Institut für Sonnenphysik, D-79104 Freiburg, Germany

³ Instituto de Astrofísica de Canarias, E-38205 La Laguna, Tenerife, Spain

⁴ Departamento de Astrofísica, Universidad de La Laguna, E-38206 La Laguna, Tenerife, Spain

⁵ Consejo Superior de Investigaciones Científicas, Spain

(Alsina Ballester et al. 2018).

Although the physical mechanism that introduces magnetic sensitivity in the Ly α scattering polarization wings is therefore not new, it is remarkable that it is capable of producing measurable effects even in a far UV line like hydrogen Ly α . This is because, at line-wing wavelengths, the ρ_V coefficient takes sizeable values relative to the absorption coefficient already when the Zeeman splitting becomes comparable to the radiative and collisional line broadening. In contrast, the signals produced by the familiar Zeeman effect depend on the ratio of the magnetic splitting over the Doppler width of the line and therefore scale with the wavelength of the spectral line under consideration.

2. FORMULATION OF THE PROBLEM

We present the results of non-local thermodynamic equilibrium (NLTE) RT calculations of the intensity and linear polarization of the hydrogen Ly α line, considering the semi-empirical model C of Fontenla et al. (1993), hereafter FAL-C. The use of this static one-dimensional (1D) solar atmospheric model allows us to isolate the influence of the magnetic field (although neglecting its possible horizontal fluctuations) from other possible symmetry-breaking mechanisms. The magnetic fields we have imposed in this model atmosphere are deterministic. Hereafter, we specify their direction by their inclination and azimuth, defined as illustrated in Figure 1 of Alsina Ballester et al. (2018). The lines of sight (LOSs) for the considered Stokes profiles are specified by $\mu = \cos \theta$, where θ is the heliocentric angle. The positive direction for Stokes Q has been taken along the Y axis (i.e., parallel to the limb for all LOSs with $\mu < 1$). In the calculations presented below, the line-broadening effect of both elastic and inelastic collisions is taken into account according to the rates presented in LL04 and Przybilla & Butler (2004), respectively. The depolarizing effect of the former has not been taken into account, after having verified numerically that its impact is negligible for this very strong chromospheric line.

The Ly α line is produced by the transition between the hydrogen levels $n = 1$ and $n = 2$. Taking the fine structure (FS) of hydrogen into account, and neglecting the contribution from forbidden transitions (under the electric dipole approximation), this line receives contributions from two FS transitions, namely those between the $^2P_{1/2}$ and $^2P_{3/2}$ FS levels of the 2P upper term and the $^2S_{1/2}$ FS level of the 2S lower term (i.e., the ground state). It has been established from previous theoretical investigations in the unmagnetized case (Belluzzi et al. 2012) that reliable calculations of the wing linear polarization of the hydrogen Ly α line must account for quantum interference between the $^2P_{1/2}$ and $^2P_{3/2}$ upper levels (i.e., J -state interference), in addition to PRD effects. An atomic model accounting for the various FS transitions between two terms, as well as for the quantum interference between different FS J -levels belonging to the same term, is generally referred to as a two-term atom (see LL04). A correct modeling of the wing scattering polarization of the Ly α line thus requires considering at least a two-term ($^2S - ^2P$) model atom.

On the other hand, observing that the FS components are very close to each other, it can be shown that, far from the line center, this line behaves in resonance scattering as a spinless two-level $0 - 1$ transition, in compliance with the principle of spectroscopic stability (PSS)⁶. The good agreement between the modeling that accounts for FS and the one that

neglects it can be clearly seen in the left panel of Figure 1, in which the scattering polarization profiles obtained by considering both a two-term ($^2S - ^2P$) and a two-level ($0 - 1$) model are compared, in the absence of magnetic fields. Unless otherwise noted, an LOS with $\mu = 0.3$ is considered in the figures presented in this work. The expected discrepancy in the line core is a clear manifestation of the depolarizing effect of the FS (e.g., LL04). Indeed, the gray area across the line-core region, appearing in several of the figures presented in this paper, indicates the spectral interval where the approximation of neglecting FS is not justified. The very small deviations found outside the line-core region are due to the approximate treatment of elastic collisions in the two-term atom calculations (see Belluzzi & Trujillo Bueno 2014).

At spectral distances from the line center that are much greater than both the Doppler width of the line and the magnetic splitting of the energy levels, the line emissivity is insensitive to both the Hanle and Zeeman effects, provided that the collisional broadening is significantly smaller than the natural width of the line (see LL04; also Appendix B of Alsina Ballester et al. 2018). For illustrative purposes, throughout this work we will focus on a wing wavelength around which the linear polarization maximizes.⁷ More precisely, we consider the wavelength at 360 mÅ to the blue of the line center (hereafter λ_m) and we point out that this spectral separation is much greater than the magnetic splitting of the energy levels, even in the presence of magnetic fields of a few kilogauss. It is also considerably larger than the Doppler width corresponding to the atmospheric regions where most of the radiation at wavelength λ_m comes from. Indeed, considering the FAL-C model, the Doppler width is approximately 55 mÅ at $z_m = 1998.5$ km; at this height the optical depth at wavelength λ_m is close to unity for an LOS with $\mu = 0.3$.

The magnetic sensitivity of the scattering polarization in the wings of this line is instead governed by the MO effects quantified by the RT coefficient ρ_V . It is important to note that the impact of such effects is only appreciable if another physical mechanism, such as scattering processes subject to PRD phenomena, produces sizable linear polarization signals outside the Doppler core (see Alsina Ballester et al. 2017). Using the two-level atomic model, we have verified that, when artificially setting ρ_V to zero, magnetic fields with strengths up to 5 kG have no impact on the line's wing linear polarization. In the right panel of Figure 1, we compare the ratio of ρ_V over the absorption coefficient η_I obtained from the two-term atom equations to that found for a $0 - 1$ two-level atom, in the presence of a horizontal magnetic field of 50 G⁸. The results of the two calculations, carried out at height z_m in the FAL-C model, present an excellent agreement, confirming the suitability of neglecting FS when modeling the magnetic sensitivity of this line's wing scattering polarization signals. As shown in Appendix B, the far-wing value of ρ_V is proportional to the spectral distance between the centers of gravity of the

Sect 10.17 of LL04): "If two different descriptions are used to characterize a quantum system – a detailed description which takes an inner quantum number into account and a simplified description which disregards it – the predicted results must be the same in all physical experiments where the structure described by the inner quantum number is unimportant."

⁷ The exact spectral position of the maximum of the linear polarization fraction has a slight dependence on the LOS and on the magnetic field under consideration.

⁸ The Hanle critical field of the hydrogen Ly α line, i.e., the magnetic field strength at which the Zeeman splitting of the level with $J = 3/2$ is equal its natural width, is approximately 53 G.

⁶ The principle of spectroscopic stability is often stated as follows (see

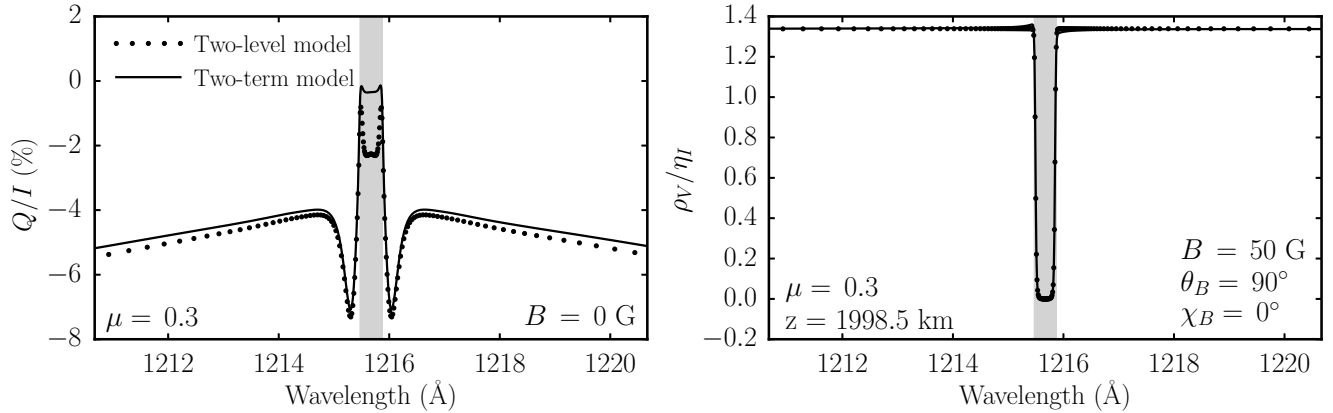


FIG. 1.— Left panel: Q/I scattering polarization pattern of the hydrogen Ly α line, modeled both as a two-term atom (solid curve) and as a spinless two-level atom (dotted curve). Results are obtained from a radiative transfer (RT) calculation, using the FAL-C model, in the absence of a magnetic field. Right panel: ρ_V/η_I ratio obtained from the same atomic models, in the presence of a 50 G horizontal magnetic field with azimuth $\chi_B = 0^\circ$, considering the FAL-C model at 1998.5 km. The gray area indicates the spectral region where the two-level approximation is not suitable.

σ_b and σ_r components of the line. Thus, the above-mentioned agreement is ultimately related to the fact that - in accordance with the PSS - the frequency shifts of the centers of gravity of the σ_b , π , and σ_r components for a two-term atom, obtained accounting for the incomplete Paschen-Back (IPB) effect, coincide with those of a normal Zeeman triplet, i.e., of a spinless two-level atomic transition (e.g., Section 3.4 of LL04).

3. THE IMPACT OF MAGNETO-OPTICAL EFFECTS

In this section, we present the results of illustrative RT calculations of the Ly α wing scattering polarization signals, considering a spinless two-level model atom and accounting for the joint impact of PRD and of magnetic fields through the Hanle, Zeeman, and MO effects. Details on the theoretical and numerical framework can be found in Alsina Ballester et al. (2017). We consider magnetic fields with a constant strength and orientation throughout the FAL-C model atmosphere, paying particular attention to vertical and horizontal (as well as nearly vertical and nearly horizontal) magnetic fields.

3.1. Linear Polarization Profiles for Deterministic Magnetic Fields

The top panels of Figure 2 show the linear polarization profiles at an LOS with $\mu = 0.3$, in the presence of horizontal ($\theta_B = 90^\circ$) magnetic fields of various strengths with azimuth $\chi_B = 0^\circ$ (this choice of azimuth maximizes the longitudinal component of the magnetic field). Outside the Doppler core, the MO effects induced by such magnetic fields produce a U/I signal and a depolarization in Q/I . The influence of such effects is controlled by the ratio of ρ_V over η_I , which depends on the longitudinal component of the magnetic field. Interestingly, this ratio scales with the same parameters that characterize the efficacy of the Hanle effect (see Appendix B). Indeed, such MO effects are expected to noticeably impact the wings of the linear polarization signals when the magnetic field strength is comparable to the Hanle critical field. Moreover, in the presence of increasingly strong magnetic fields, the impact of such MO effects is appreciable in the wings of both Q/I and U/I at greater spectral distances from the line center. As pointed out in Alsina Ballester et al. (2018), the relative contribution of continuum processes to η_I is greater farther into the line wings, implying that stronger magnetic fields are required in order for the ρ_V/η_I ratio to be significant. Note also that, in addition to their amplitude, also the

sign of the U/I wing signals is sensitive to the orientation of the magnetic field. For instance, comparing horizontal magnetic fields with $\chi_B = 0^\circ$ and $\chi_B = 180^\circ$, which have longitudinal components of the same magnitude but point in the opposite direction, we have verified that the depolarization of Q/I is the same, while the resulting U/I wing signal is identical in absolute value but with opposite sign. We point out that, because the wing Q/I scattering polarization signals are negative in the unmagnetized case, the MO effects induced by a magnetic field with a positive (negative) longitudinal component give rise to negative (positive) U/I signals.

We have also considered the case of vertical magnetic fields ($\theta_B = 0^\circ$) of increasing strength, for an LOS with $\mu = 0.3$. As seen in the bottom left panel of Figure 2, for $B = 300$ G the wings of Q/I are almost completely depolarized within a ± 5 Å spectral range around line center, and a significant depolarization is also appreciable much farther into the wings. These profiles have a strong resemblance to those obtained in the presence of a horizontal magnetic field of 100 G discussed above. This can be easily understood by observing that the longitudinal components of the two aforementioned field configurations are very similar (around 90 G). Interestingly, in the presence of magnetic fields with such longitudinal components, the near wings of the U/I profiles still have a considerable amplitude (see the right panels of Figure 2), and stronger magnetic fields are required in order for them to be considerably depolarized. Indeed, we have checked that the absolute value of the U/I wing signal at λ_m does not fall below 0.1% until magnetic fields with longitudinal components larger than 900 G are considered. Finally, just as in the case of a horizontal magnetic field, we have also verified that if the vertical magnetic field is oriented in the opposite direction (i.e., $\theta_B = 180^\circ$), the resulting depolarization of Q/I is the same and the U/I profile has the opposite sign, again as a consequence of the sign reversal of the LOS projection of the magnetic field.

The previously discussed signatures of the MO effects, namely the depolarization of Q/I together with the appearance of a U/I signal whose sign depends on the orientation of the magnetic field, offer a new tool for inferring the longitudinal component of the magnetic fields in the chromospheric regions where the Ly α wings originate. The magnetic sensitivity of this line's wing scattering polarization signals can be expected to be well above the noise level, even in quiet regions of the solar atmosphere where the circular polarization

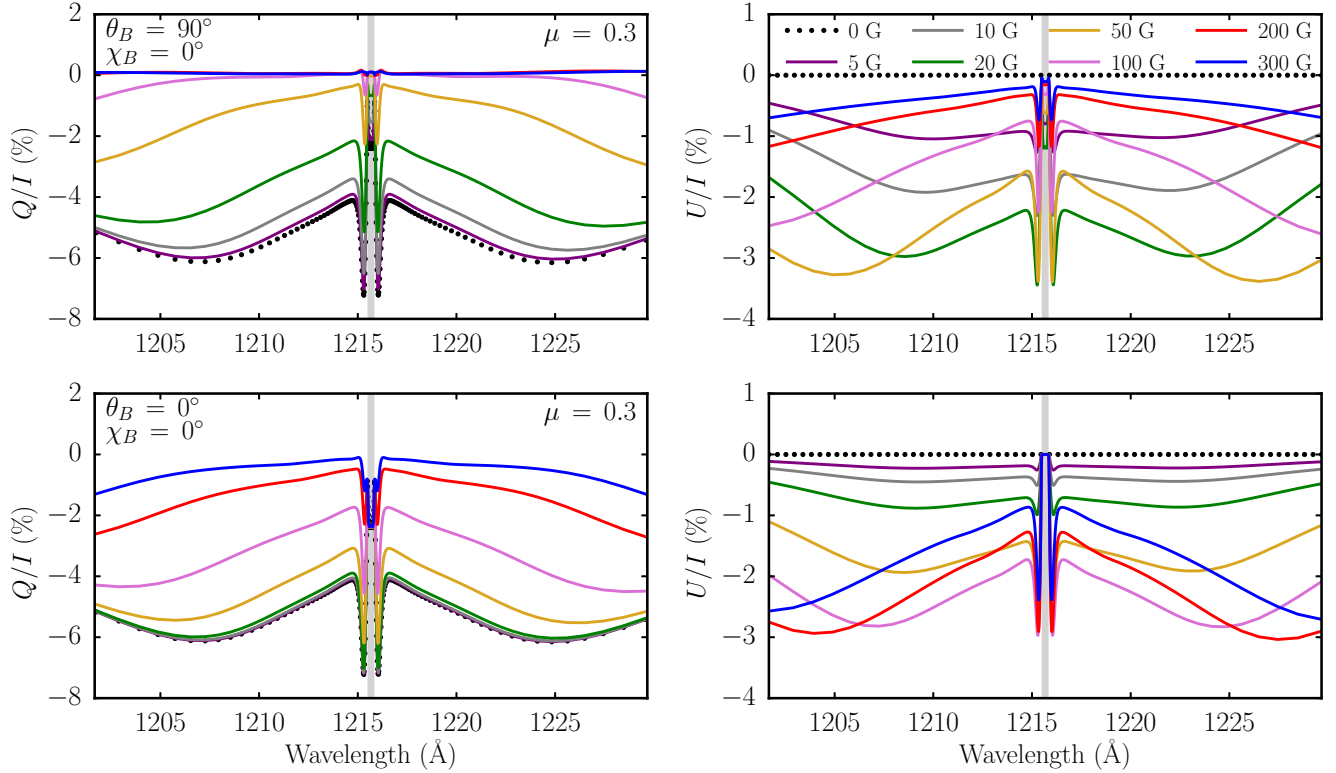


FIG. 2.— The Stokes Q/I (left panels) and U/I (right panels), calculated in the presence of both horizontal ($\theta_B = 90^\circ$) magnetic fields with azimuth $\chi_B = 0^\circ$ (top panels) and vertical ($\theta_B = 0^\circ$) magnetic fields (bottom panels). The colored curves (see the legend) correspond to the various considered field strengths. The black dotted curves represent the unmagnetized reference case. When considering horizontal magnetic fields with the same strengths but with azimuth $\chi_B = 180^\circ$ (not shown), the resulting Q/I profiles coincide exactly with those shown for horizontal magnetic fields with $\chi_B = 0^\circ$, while the corresponding curves for U/I are identical in absolute value but opposite in sign. Likewise, the Q/I profiles obtained in the presence of vertical downward-pointing magnetic fields ($\theta_B = 180^\circ$; not shown) coincide with those with $\theta_B = 0^\circ$ and a sign reversal is found in the U/I profiles.

signals produced by the Zeeman effect would be extremely weak. Moreover, the scattering polarization signal is clearly appreciable very far into the line wings, thus encoding information on the magnetic activity in deeper chromospheric layers.

3.2. Center-to-limb Variation for Deterministic Magnetic Fields

Figures 3 and 4 show the center-to-limb variation (CLV) of the Q/I and U/I signals at λ_m , calculated for nearly vertical ($\theta_B = 20^\circ$; Figure 3) and nearly horizontal ($\theta_B = 70^\circ$; Figure 4) magnetic fields of various strengths up to 300 G, both for $\chi_B = 0^\circ$ and $\chi_B = 180^\circ$.

The CLV for Q/I and U/I found in the presence of magnetic fields with $\theta_B = 20^\circ$ and $\chi_B = 0^\circ$ can be explained in a relatively straightforward manner. The projection of the magnetic field along the LOS – and therefore the value of ρ_V/η_I – has the same sign for all μ between 0 and 1 and increases monotonically up to $\mu \approx 0.94$. As the magnetic field strength increases, one finds a progressively greater departure from the $(1 - \mu^2)$ trend for Q/I , theoretically predicted in the unmagnetized case. The amplitude of the U/I signals, produced by the same MO effects, is found to decrease monotonically with μ , because it depends on both the longitudinal component of the magnetic field and the amplitude of the Q/I signals. The U/I signals increase in amplitude with the field strength up to roughly 50 G, but for even stronger fields they begin to decrease, as the MO effects produce a net reduction of the total fraction of linear polarization (see Appendix A of Alsina

Ballester et al. 2018).

The situation is substantially different in the presence of magnetic fields with $\theta_B = 20^\circ$ and $\chi_B = 180^\circ$ (see the bottom panels of Figure 3). In this case, the magnetic field points away from the observer for LOSs with small μ values, it becomes completely transversal at $\mu \approx 0.34$, and its longitudinal component becomes positive and increases as one continues approaching $\mu = 1$. Compared to the case in which $\chi_B = 0^\circ$, the longitudinal component is smaller when considering LOSs with small μ values, resulting in a much more modest depolarization in Q/I , especially around the LOS at which the magnetic field is transversal. It is interesting to note that, even at this LOS, the magnetic field still produces some depolarization, despite the fact that ρ_V is zero in this direction. This can be explained because the pumping radiation field is nevertheless modified by MO effects, thereby impacting the linear polarization emitted in this direction (e.g., Alsina Ballester et al. 2016, 2018). There are also clear qualitative differences with respect to the previous case in the CLV for U/I ; in this case their signals are positive for LOS with large inclinations and become negative when directions closer to the vertical are considered. The sign inversion occurs around the LOS for which such fields are transversal, although the exact μ value changes with the field strength because of modification of the pumping radiation field induced by MO effects.

On the other hand, when considering nearly horizontal ($\theta_B = 70^\circ$) magnetic fields (see Figure 4), the CLV obtained in the presence of fields with $\chi_B = 0^\circ$ and $\chi_B = 180^\circ$ are qualitatively very similar to each other. Nevertheless, is worth

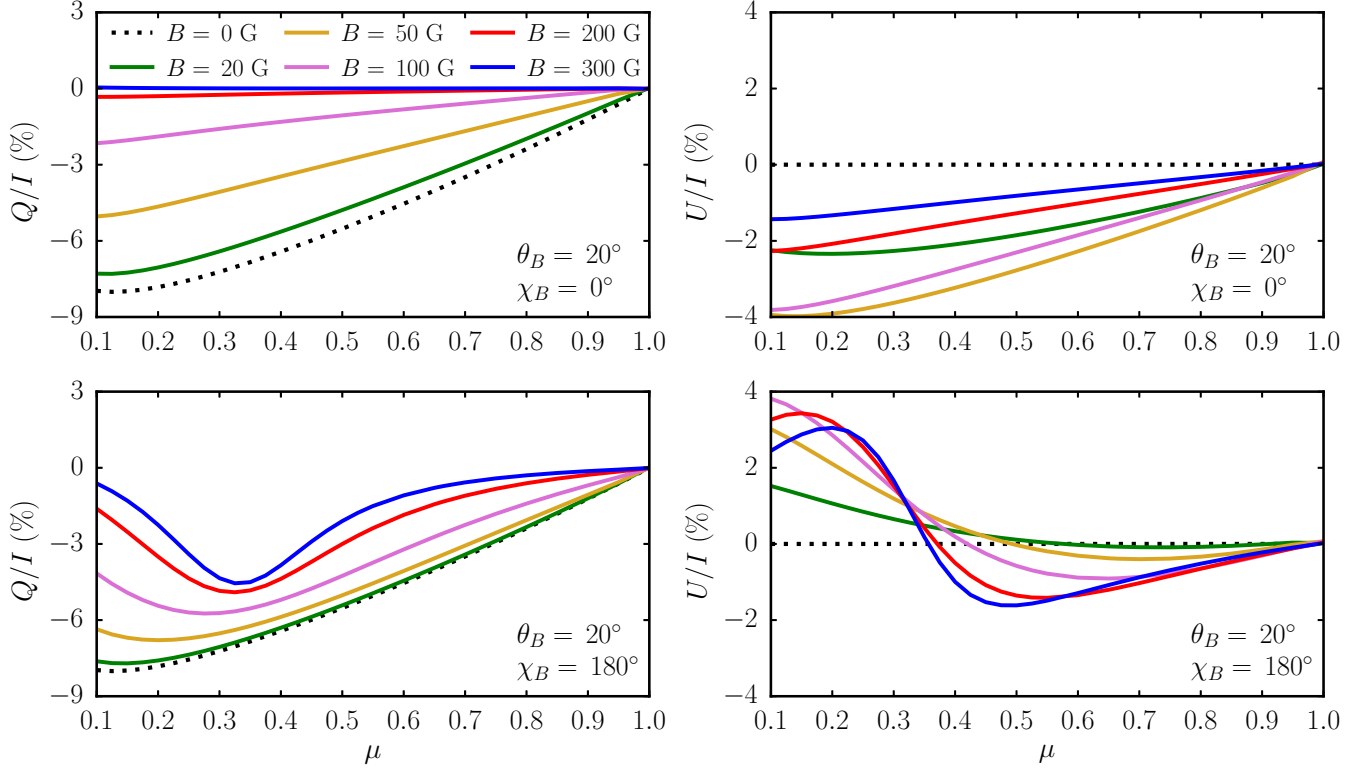


Fig. 3.— Center-to-limb variation (CLV) of the Q/I (left panels) and U/I (right panels) wing signals obtained at $360 \text{ m}\text{\AA}$ to the blue of line center (i.e., the λ_m wavelength defined in the text), for magnetic fields with inclination $\theta_B = 20^\circ$ and azimuths $\chi_B = 0^\circ$ (top panels) and $\chi_B = 180^\circ$ (bottom panels). The colored curves (see the legend) correspond to various field strengths up to 300 G. The black dotted curves represent the reference unmagnetized case.

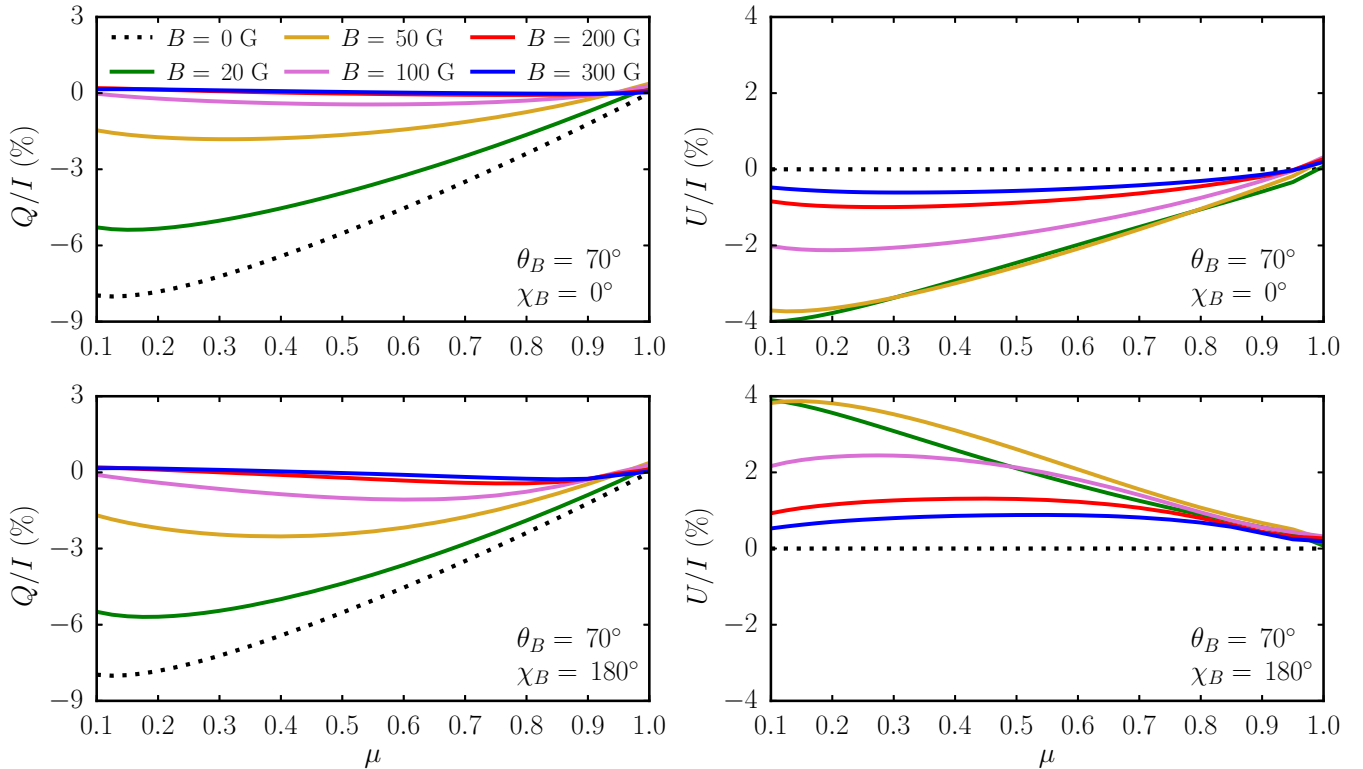


Fig. 4.— Same as the previous figure, but in the presence of magnetic fields with inclination $\theta_B = 70^\circ$.

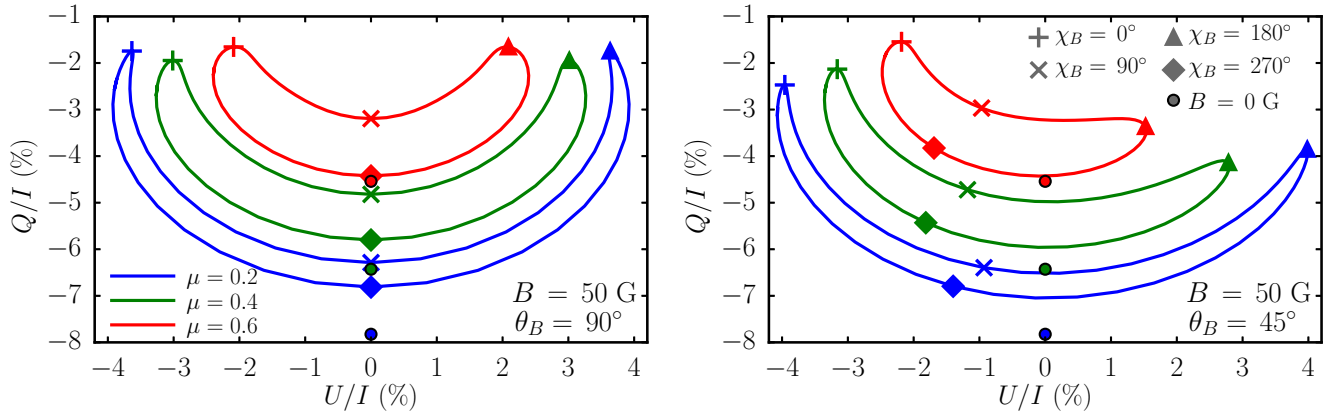


FIG. 5.— Polarization diagrams for magnetic fields of 50 G, with inclinations of $\theta_B = 90^\circ$ (left panel) and 45° (right panel). Each closed curve represents the change in scattering polarization with azimuth, for LOS with $\mu = 0.2$ (blue curves), $\mu = 0.4$ (green curves), and $\mu = 0.6$ (red curves). The various markers indicate specific azimuths (see legend), except for the circles, which represent the unmagnetized reference case.

noting that, for LOSs with small μ values, the longitudinal component of the magnetic field – and thus the depolarization of Q/I – is slightly greater for the former case than for the latter. For small μ , such nearly horizontal magnetic fields give rise to a considerably stronger depolarization than those with an inclination of $\theta_B = 20^\circ$, also in this case due to their larger longitudinal components.

3.3. A Look at Observational Data: CLASP

Recently, CLASP successfully measured the linear polarization signals of the Ly α line emerging from quiet regions of the Sun, spanning from off-limb positions to close to the disk center (see Kano et al. 2017). In the wings of the Q/I and U/I profiles, considerable fluctuations along the spatial direction of the radially oriented slit were found. The amplitude of the wing Q/I signal was found to decrease with μ (in agreement with our theoretical expectations), while no serious CLV was observed in the amplitude of U/I . We are confident that the observed lack of CLV in the U/I wing signals can be explained by accounting for horizontal variations in the longitudinal component of the magnetic field, which could substantially modify the net amplitude of the signals resulting from MO effects, and/or by the axial asymmetries in other thermodynamical properties of the solar atmosphere, which may produce U/I signals of non-magnetic origin. An accurate modeling of the scattering polarization signals observed in strong resonance lines such as H I Ly α must therefore account for the full three-dimensional complexity of the solar atmosphere, as well as the joint action of scattering polarization with PRD phenomena and the Hanle, Zeeman, and MO effects.

In spite of the simplification that the FAL-C semi-empirical model implies, it is worthwhile to note that the results of our radiative transfer calculations in this 1D model of the solar atmosphere can be invoked to qualitatively explain one of the other spectacular observational results provided by CLASP. In addition to the wavelength variation of the linear polarization profiles, CLASP provided Stokes I and Stokes Q/I broadband images over a large field of view (see Kano et al. 2017). Within this field of view there was a bright plage and a multitude of network and inter-network features. Interestingly, the bright plage region and some of the network features that can be distinguished in the Stokes I image show nearly zero linear polarization in the Stokes Q/I image, while the surrounding quiet regions instead show very significant polarization signals. In a forthcoming publication we will in-

vestigate whether this can be explained on the basis of the results reported above, by noting that the broadband Q/I signals observed by CLASP are dominated by the linear polarization in the Ly α wings (see Belluzzi et al. 2012) and by bearing in mind that plages and the network have stronger magnetic fields than the surrounding quieter regions.

3.4. Unresolved Magnetic Fields

Further insights into the magnetic sensitivity of the linear polarization in the wings can be gained by studying its behavior on the $Q/I - U/I$ plane. The closed curves in the polarization diagrams shown in Figure 5 indicate how the fractional linear polarization signals obtained at λ_m change with χ_B in the presence of 50 G magnetic fields with a fixed inclination. The diagram is symmetric around the $U/I = 0$ axis for $\theta_B = 90^\circ$ (left panel), but this is not the case for arbitrary inclinations, implying the following (see Alsina Ballester et al. 2018). If one measures the net U/I to be zero in a given spatially unresolved region of the solar atmosphere, this is an indication that the magnetic field therein is transversal, or otherwise has a distribution such that the averaged longitudinal component is zero⁹.

We also point out that magnetic field distributions that do not fulfil the aforementioned condition are capable of producing a net U/I signal even if their orientations change at scales below the mean free path of the line’s photons (i.e., microstructured magnetic fields). Indeed, for such a field configuration, in which the inclination is fixed and the azimuth changes randomly, the ρ_V is generally not zero (see Equations (6b) and (50a) of Alsina Ballester et al. 2017), implying that a U/I signal may be produced in the wings. By contrast, for the same field configuration the Hanle effect may modify the line-core Q/I amplitude of the scattered radiation, but it produces no U/I signal (see Eqs. (11), (21), (22), and (50b) of the same paper). Such qualitative differences can be understood by realizing that the MO effects quantified by ρ_V depend only on the net longitudinal component of the magnetic field, which is only zero for all LOSs if $\theta_B = 90^\circ$. On the other hand, the Hanle effect also depends on the angle between the magnetic

⁹ From symmetry considerations it can be seen that the two following possible scenarios fulfil this condition: (a) a magnetic field distribution with axial symmetry around a given axis that is perpendicular to the LOS, and (b) a distribution with axial symmetry around any given axis, having also reflective symmetry with respect to the plane normal to the same axis. The configuration presented in the left panel of Figure 5 is a particular case of the latter.

field and the symmetry axis of the pumping radiation field, which in a 1D unmagnetized atmospheric model is parallel to the local vertical. The field configuration discussed here is symmetric around this axis and, as a result, the Hanle effect does not cause a rotation of the plane of linear polarization of the scattered radiation, although it may decrease the degree of linear polarization.

4. CONCLUDING COMMENTS

Motivated by the recent theoretical discovery that the wing scattering polarization of some strong resonance lines is highly sensitive to the MO effects quantified by the ρ_V terms of the transfer equations for Stokes Q and U , we have conducted an RT investigation on the wing linear polarization signals of the hydrogen Ly α line. We have modeled this line considering a spinless two-level atom (i.e., the impact of FS has been neglected), having shown that this approximation is suitable outside the Doppler core. We have found that the wing scattering polarization signals of this far UV line are in fact sensitive to longitudinal magnetic fields, even when they are considerably weaker than the Hanle critical field.

Such signals extend far into the line wings, potentially offering a method to simultaneously infer the LOS components of the magnetic fields present in a wide range of depths throughout the solar chromosphere. The sign of such components can be determined from that of U/I , while the combined amplitude of Q/I and U/I are indicative of their magnitude. From symmetry considerations applied to the polarization di-

agrams, we conclude that measuring a nonzero U/I wing signal may be a signature of an asymmetry of the distribution of the LOS component of the magnetic field within the considered spatial resolution element.

This investigation reveals that relatively weak magnetic fields may strongly impact the wing scattering polarization signals of the Ly α line via MO effects. Interestingly, the broadband Q/I images provided by the CLASP suborbital rocket experiment revealed linear polarization signals close to zero in the regions of the field of view corresponding to a plage and to some of the network features, in contrast to the much less magnetized surrounding regions. As we shall show in detail in a forthcoming publication, these observations can potentially be explained on the basis of the depolarization that MO effects produce in the wings of the Ly α line.

Finally, we emphasize that an accurate RT modeling of the scattering polarization in the hydrogen Ly α line requires accounting for the 3D structure of the solar atmosphere, in addition to the joint action of resonance scattering with PRD and the Hanle, Zeeman, and MO effects.

E.A.B. and L.B. gratefully acknowledge financial support by the Swiss National Science Foundation (SNSF) through Grant 200021_175997. J.T.B. acknowledges the funding received from the European Research Council (ERC) under the European Union's Horizon 2020 research and innovation programme (ERC Advanced Grant agreement No. 742265).

APPENDIX

A. THE FAR-WING LIMIT OF THE ELEMENTS OF THE PROPAGATION MATRIX

Here we present an analytical study of the magnetic dependence of the elements of the line contribution to the so-called propagation matrix (see LL04), focusing on spectral regions far beyond the Doppler core. We consider a two-term atomic model without hyperfine structure, in the presence of magnetic fields of arbitrary strength. In order to determine the various eigenstates of an atomic system in the presence of an external magnetic field, one must diagonalize the total Hamiltonian $H = H_0 + H_B$, in which H_0 is the Hamiltonian of the unperturbed atomic system and H_B is the magnetic Hamiltonian (see Condon & Shortley 1935). Taking the quantization axis of total angular momentum J (i.e., the z -axis) parallel to the magnetic field, the magnetic Hamiltonian obeys the following commutation rules,

$$[H_B, J_z] = 0, \quad [H_B, J_x] \neq 0, \quad [H_B, J_y] \neq 0.$$

Therefore, in the presence of a magnetic field the quantum number J generally loses the property of being a ‘‘good’’ quantum number, while this property is preserved for the quantum number M . When the magnetic energy is much smaller than the energy intervals of H_0 the effect of H_B can be computed through a perturbative approach to first order (e.g., Landi Degl’Innocenti 2014), which implies its diagonalization over the degenerate eigenvectors of H_0 . The matrix $\langle \beta LS JM | H_B | \beta LS JM' \rangle$ is diagonal and the magnetic field produces an energy splitting of the magnetic sublevels that scales linearly with the field strength. This approach is commonly known as the linear Zeeman splitting approximation (LZS). In the more general case, commonly referred to as the IPB effect regime, when performing the diagonalization of the total Hamiltonian on the basis $|\beta LS JM\rangle$, one finds that the magnetic field produces a mixing of the various J -levels. The ensuing eigenvectors are characterized by quantum number M as well as by the label j :

$$\begin{aligned} H |\beta_u L_u S j_u M_u\rangle &= E_{j_u}(\beta_u L_u S, M_u) |\beta_u L_u S j_u M_u\rangle; & |\beta_u L_u S j_u M_u\rangle &= \sum_{J_u} C_{J_u}^{j_u}(\beta_u L_u S, M_u) |\beta_u L_u S J_u M_u\rangle, \\ H |\beta_\ell L_\ell S j_\ell M_\ell\rangle &= E_{j_\ell}(\beta_\ell L_\ell S, M_\ell) |\beta_\ell L_\ell S j_\ell M_\ell\rangle; & |\beta_\ell L_\ell S j_\ell M_\ell\rangle &= \sum_{J_\ell} C_{J_\ell}^{j_\ell}(\beta_\ell L_\ell S, M_\ell) |\beta_\ell L_\ell S J_\ell M_\ell\rangle, \end{aligned}$$

where the u and ℓ subscripts refer to the states of the upper and lower term, respectively. $E_j(\beta LS, M)$ is the energy for each eigenstate and the $C_j^j(\beta LS, M)$ coefficients describe the coupling between such states and the $|\beta LS JM\rangle$ basis eigenvectors. Given that the sum of the eigenvalues of a Hamiltonian are equal to its trace, it can be shown that for each term

$$\sum_{jM} E_j(\beta LS, M) = n E(\beta LS),$$

where n is the number of different eigenstates belonging to the considered term and $E(\beta LS)$ is the energy of the term. Each of the (electric-dipole) radiative transitions between the various states of the upper term $|\beta_u L_u S j_u M_u\rangle$ and those of the lower term

$|\beta_\ell L_\ell S j_\ell M_\ell\rangle$ are characterized by their frequencies

$$\nu_{j_u M_u, j_\ell M_\ell} = [E_{j_u}(\beta_u L_u S, M_u) - E_{j_\ell}(\beta_\ell L_\ell S, M_\ell)]/h, \quad (\text{A1})$$

where h is the Planck constant. These frequencies can also be expressed as shifts with respect to the reference frequency of the multiplet $\nu_0 = [E(\beta_u L_u S) - E(\beta_\ell L_\ell S)]/h$, in units of the Doppler width $\Delta\nu_D$, as

$$x_{j_u M_u, j_\ell M_\ell} = \frac{\nu_{j_u M_u, j_\ell M_\ell} - \nu_0}{\Delta\nu_D}. \quad (\text{A2})$$

Introducing also the reduced frequency

$$x = \frac{\nu_0 - \nu}{\Delta\nu_D}, \quad (\text{A3})$$

we note that $x_{j_u M_u, j_\ell M_\ell} + x = (\nu_{j_u M_u, j_\ell M_\ell} - \nu)/\Delta\nu_D$. Moreover, it can easily be shown that

$$\sum_{j_u M_u, j_\ell M_\ell} x_{j_u M_u, j_\ell M_\ell} = 0. \quad (\text{A4})$$

The various transitions between the upper and lower term can be divided into three groups according to $\Delta M \equiv (M_u - M_\ell) = (\pm 1, 0)$. Following the terminology generally used in the literature, we refer to the groups with $q = -\Delta M = (-1, 0, 1)$ as the σ_r , π , and σ_b components, respectively. The strength of each transition is given by (see LL04)

$$S_q^{j_u M_u, j_\ell M_\ell} = \frac{3}{2S+1} \sum_{J_u J'_u} C_{J_u}^{j_u}(\beta_u L_u S, M_u) C_{J'_u}^{j_u}(\beta_u L_u S, M_u) \sum_{J_\ell J'_\ell} C_{J_\ell}^{j_\ell}(\beta_\ell L_\ell S, M_\ell) C_{J'_\ell}^{j_\ell}(\beta_\ell L_\ell S, M_\ell) \\ \times \sqrt{(2J_u+1)(2J'_u+1)(2J_\ell+1)(2J'_\ell+1)} \begin{Bmatrix} J_u & J_\ell & 1 \\ L_\ell & L_u & S \end{Bmatrix} \begin{Bmatrix} J'_u & J'_\ell & 1 \\ L_u & L_\ell & S \end{Bmatrix} \begin{pmatrix} J_u & J_\ell & 1 \\ -M_u & M_\ell & -q \end{pmatrix} \begin{pmatrix} J'_u & J'_\ell & 1 \\ -M_u & M_\ell & -q \end{pmatrix}, \quad (\text{A5})$$

which fulfil the following normalization condition

$$\sum_{j_u M_u, j_\ell M_\ell} S_q^{j_u M_u, j_\ell M_\ell} = 1, \quad q = (-1, 0, 1). \quad (\text{A6})$$

As discussed in this paper, under the electric-dipole approximation the H I Lyman- α line can be modeled as a two-term atom whose upper term has two FS levels, $^2P_{1/2}$ and $^2P_{3/2}$. Relative to the ground state, their energies are $82258.919 \text{ cm}^{-1}$ and $82259.285 \text{ cm}^{-1}$, respectively. Considering field strengths of up to 500 G, we have verified that the $x_{j_u M_u, j_\ell M_\ell}$ frequency shifts calculated making the LZS approximation present a very good agreement with those obtained in the general IPB effect regime, as is shown in the left panels of Figure 6. The quality of this agreement should not be surprising, because the energy separation between the FS levels of the upper term is more than one order of magnitude larger than the splitting between M -levels induced by a magnetic field of such strength.

On the other hand, we note that when the LZS approximation is made, the $C_j^j(\beta L S, M)$ coefficients reduce to $\delta_{j,j}$ and the magnetic dependence of the transition strengths given in Equation (A5) completely vanishes. This contrasts with the results obtained in the IPB effect regime, in which the transition strengths are appreciably modified by such weak magnetic fields, as is shown in the right panels of Figure 6.

The frequencies of the centers of gravity of the σ_b , π , and σ_r groups, relative to ν_0 and in units of Doppler width are defined as

$$\bar{x}_q = \sum_{j_u M_u, j_\ell M_\ell} S_q^{j_u M_u, j_\ell M_\ell} x_{j_u M_u, j_\ell M_\ell}. \quad (\text{A7})$$

For the discussions below, it will also be useful to introduce $\bar{\nu}_q \equiv \bar{x}_q \Delta\nu_D$. It can be shown that, for a two-term atomic model in the IPB effect regime, the frequency shifts of the centers of gravity of the three groups scale linearly with the strength of the magnetic field (see LL04), according to

$$\bar{x}_q = -q \frac{\nu_L}{\Delta\nu_D}, \quad (\text{A8})$$

in which we have introduced the Larmor frequency $\nu_L = \mu_0 B/h$, where μ_0 is the Bohr magneton. Such frequency shifts coincide with those for a spinless two-level atomic model. On the other hand, such shifts are considerably overestimated when the LZS approximation is made (see Figure 7), as a consequence of neglecting the magnetic dependence of the strengths of the various transitions. The necessity of fully accounting for the IPB effect in order to correctly determine the spectral positions of the centers of gravity, also in the presence of magnetic fields weak enough that the splitting they induce is much smaller than separation between FS levels, was already pointed out by Socas-Navarro et al. (2004).

The explicit expressions for the elements of the propagation matrix for a two-term atom with an unpolarized lower term, in the presence of a magnetic field of arbitrary strength, can be obtained as a particular case of those for a multi-term atom given in Section 7.6 of LL04. For the the purposes of this work, it is convenient to write such coefficients (defined taking the quantization

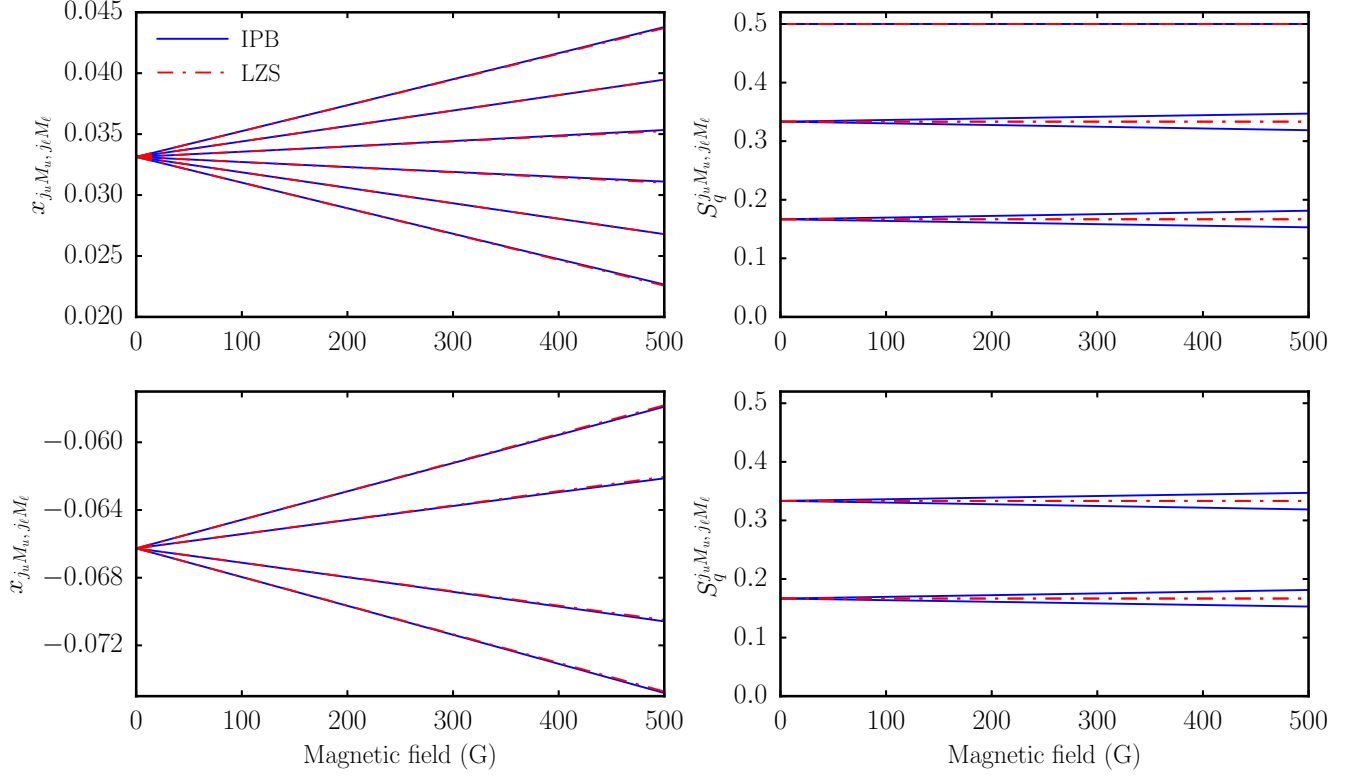


FIG. 6.— Left panels: reduced frequency shifts (see Equation (A2)) for the various transitions between the upper (2P) and lower (2S) term of the Ly α line, as a function of magnetic field strength. The Doppler width has been taken at a height of 1998.5 km in the FAL-C atmospheric model, corresponding to 54.4 m \AA . Right panels: normalized strengths for the same transitions (see Equation (A5)), as a function of magnetic field strength. The top (bottom) panels illustrate the transitions whose upper state has total angular momentum $J_u = 3/2$ ($J_u = 1/2$) in the absence of magnetic field. The black solid curves represent the results of the calculation accounting for the incomplete Paschen-Back effect, while those represented by the red dashed-dotted curves are obtained under the linear Zeeman splitting approximation. Note that several of the curves corresponding to the strengths of different transitions may overlap.

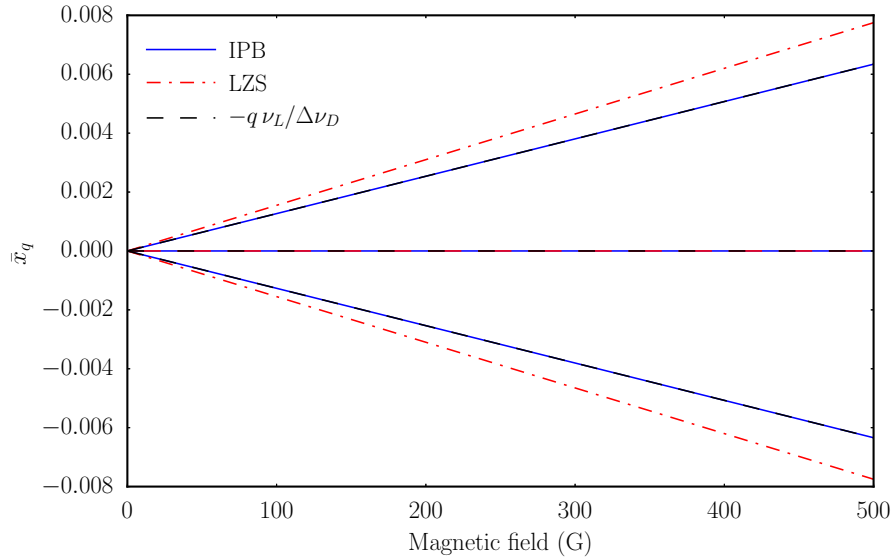


FIG. 7.— Spectral positions of the centers of gravity (see Equation (A7)), taking a two-term atomic model for the H I Ly α line. The Doppler width has been taken at a height of 1998.5 km in the FAL-C atmospheric model, corresponding to 54.4 m \AA . The blue solid lines represent the spectral positions obtained in the incomplete Paschen-Back effect regime, the red dashed-dotted lines represent the same values obtained under the linear Zeeman splitting approximation, and the black dashed lines follow Equation (A8).

axis parallel to the magnetic field), for a given frequency ν and direction $\mathbf{\Omega}$ as

$$\eta_i(\nu, \mathbf{\Omega}) = k_M \sum_K \sqrt{\frac{2K+1}{3}} \mathcal{T}_0^K(i, \mathbf{\Omega}) \sum_q (-1)^{1+q} \begin{pmatrix} 1 & 1 & K \\ q & -q & 0 \end{pmatrix} \phi_q(\nu), \quad (i = 0, 1, 2, 3) \quad (\text{A9})$$

$$\rho_i(\nu, \mathbf{\Omega}) = k_M \sum_K \sqrt{\frac{2K+1}{3}} \mathcal{T}_0^K(i, \mathbf{\Omega}) \sum_q (-1)^{1+q} \begin{pmatrix} 1 & 1 & K \\ q & -q & 0 \end{pmatrix} \psi_q(\nu), \quad (i = 1, 2, 3) \quad (\text{A10})$$

where k_M is the so-called frequency-integrated absorption coefficient and $\mathcal{T}_0^K(i, \mathbf{\Omega})$ are the polarization tensors introduced in Landi Degl'Innocenti (1983). The ϕ_q and ψ_q profiles appearing in the previous expression are given by

$$\phi_q(\nu) = \sum_{j_u M_u, j_\ell M_\ell} S_q^{j_u M_u, j_\ell M_\ell} \text{Re}\{\Phi(\nu_{j_u M_u, j_\ell M_\ell} - \nu)\}; \quad \psi_q(\nu) = \sum_{j_u M_u, j_\ell M_\ell} S_q^{j_u M_u, j_\ell M_\ell} \text{Im}\{\Phi(\nu_{j_u M_u, j_\ell M_\ell} - \nu)\}. \quad (\text{A11})$$

In the proofs presented hereafter, we consider the observer's reference frame, making the assumption that the distribution of atomic velocities is Maxwellian. In terms of reduced frequencies, the complex absorption profiles $\Phi(\nu_{j_u M_u, j_\ell M_\ell} - \nu)$ introduced above can be given as

$$\Phi(\nu_{j_u M_u, j_\ell M_\ell} - \nu) = \frac{1}{\sqrt{\pi} \Delta \nu_D} \left(H(x + x_{j_u M_u, j_\ell M_\ell}, a) + i L(x + x_{j_u M_u, j_\ell M_\ell}, a) \right), \quad (\text{A12})$$

where H and L are the Voigt profile and the associated dispersion profile, respectively (see LL04 for their explicit expressions). They contain the damping parameter $a = \Gamma/(4\pi\Delta\nu_D)$, where Γ is the line-broadening parameter. Note that $\Gamma = \Gamma_R + \Gamma_E + \Gamma_I$, where Γ_R is the radiative de-excitation rate, which corresponds to the Einstein coefficient for spontaneous emission $A(\beta_u L_u S \rightarrow \beta_\ell L_\ell S)$, and Γ_I and Γ_E are the de-excitation rates due to inelastic and elastic collisions, respectively. The discussion presented below concerns frequencies far from line center, for which the condition $x^2 + a^2 \gg 1$ is fulfilled and so one can take the asymptotic expansion (see LL04) for the H and L to the lowest order in x ,

$$H(x, a) \sim \frac{1}{\sqrt{\pi}} \frac{a}{x^2 + a^2}, \quad L(x, a) \sim \frac{1}{\sqrt{\pi}} \frac{x}{x^2 + a^2}. \quad (\text{A13})$$

B. PARTICULAR CASE: THE TWO-LEVEL ATOM FOR A 0 – 1 TRANSITION

Before considering a two-term atomic model with arbitrary values for L_u , L_ℓ , and S , let us first consider the particular case in which $S = 0$ so that $J_u = L_u$ and $J_\ell = L_\ell$ (corresponding to the case of a two-level atomic model). In a reference frame such that the quantization axis is taken along the direction of the magnetic field, the elements of the propagation matrix given in Eqs. (A9) and (A10) can be written in a more compact form by introducing the generalized profile $\Phi_Q^{K,K'}$ and the generalized dispersion profile $\Psi_Q^{K,K'}$ (e.g., Landi Degl'Innocenti et al. 1991), yielding

$$\eta_i(x, \mathbf{\Omega}) = k_M \sum_K \mathcal{T}_0^K(i, \mathbf{\Omega}) \Phi_0^{0,K}(J_\ell, J_u, x), \quad \rho_i(x, \mathbf{\Omega}) = k_M \sum_K \mathcal{T}_0^K(i, \mathbf{\Omega}) \Psi_0^{0,K}(J_\ell, J_u, x). \quad (\text{B1})$$

By selecting the reference direction for positive Stokes Q so that the η_U and ρ_U coefficients are zero, the previous expression can be given explicitly in terms of the angle α between the direction of propagation and the magnetic field as

$$\begin{aligned} \eta_I(x, \mathbf{\Omega}) &= k_M \left(\Phi_0^{0,0}(J_\ell, J_u; x) + \frac{\sqrt{2}}{4} (3 \cos^2 \alpha - 1) \Phi_0^{0,2}(J_\ell, J_u; x) \right), \\ \eta_Q(x, \mathbf{\Omega}) &= k_M \frac{3\sqrt{2}}{4} \sin^2 \alpha \Phi_0^{0,2}(J_\ell, J_u; x), & \rho_Q(x, \mathbf{\Omega}) &= k_M \frac{3\sqrt{2}}{4} \sin^2 \alpha \Psi_0^{0,2}(J_\ell, J_u; x). \\ \eta_V(x, \mathbf{\Omega}) &= k_M \frac{\sqrt{6}}{2} \cos \alpha \Phi_0^{0,1}(J_\ell, J_u; x), & \rho_V(x, \mathbf{\Omega}) &= k_M \frac{\sqrt{6}}{2} \cos \alpha \Psi_0^{0,1}(J_\ell, J_u; x). \end{aligned} \quad (\text{B2})$$

Taking also $J_u = 1$ and $J_\ell = 0$, as in the two-level model considered in previous sections, the generalized profiles and generalized dispersion profiles can be written as

$$\begin{aligned} \Phi_0^{0,0}(0, 1; x) &= \frac{1}{3} [\phi_1 + \phi_0 + \phi_{-1}], & \Phi_0^{0,1}(0, 1; x) &= \frac{\sqrt{6}}{6} [\phi_1 - \phi_{-1}], & \Phi_0^{0,2}(0, 1; x) &= \frac{\sqrt{2}}{6} [\phi_1 - 2\phi_0 + \phi_{-1}] \\ \Psi_0^{0,0}(0, 1; x) &= \frac{1}{3} [\psi_1 + \psi_0 + \psi_{-1}], & \Psi_0^{0,1}(0, 1; x) &= \frac{\sqrt{6}}{6} [\psi_1 - \psi_{-1}], & \Psi_0^{0,2}(0, 1; x) &= \frac{\sqrt{2}}{6} [\psi_1 - 2\psi_0 + \psi_{-1}]. \end{aligned} \quad (\text{B3})$$

We note that, for such a two-level atomic model, the transition strengths introduced in Equation (A5) can simply be written as

$$S_q^{M_u, M_\ell} = 3 \begin{pmatrix} J_u & J_\ell & 1 \\ -M_u & M_\ell & -q \end{pmatrix}^2. \quad (\text{B4})$$

Therefore, one can easily see that, in the case that $J_u = 1$ and $J_\ell = 0$, the profiles ϕ_q and ψ_q given in Equation (A11) can also be given in the following, more compact, form:

$$\phi_q = \frac{1}{\sqrt{\pi}\Delta\nu_D} H(x + \bar{x}_q, a), \quad \psi_q = \frac{1}{\sqrt{\pi}\Delta\nu_D} L(x + \bar{x}_q, a).$$

Using these expressions for the ϕ_q and ψ_q profiles together with Equation (A13), valid when considering spectral regions far from the line core, one can write the generalized profiles and generalized dispersion profiles as a sum of fractions of polynomials as

$$\Phi_0^{0,0}(0, 1; x) \sim \frac{a}{3\pi\Delta\nu_D} \left[\frac{1}{a^2 + (x + \bar{x}_1)^2} + \frac{1}{a^2 + x^2} + \frac{1}{a^2 + (x + \bar{x}_{-1})^2} \right], \quad (\text{B5})$$

$$\Phi_0^{0,1}(0, 1; x) \sim \frac{\sqrt{6}a}{6\pi\Delta\nu_D} \left[\frac{1}{a^2 + (x + \bar{x}_1)^2} - \frac{1}{a^2 + (x + \bar{x}_{-1})^2} \right], \quad (\text{B6})$$

$$\Phi_0^{0,2}(0, 1; x) \sim \frac{\sqrt{2}a}{6\pi\Delta\nu_D} \left[\frac{1}{a^2 + (x + \bar{x}_1)^2} - \frac{2}{a^2 + x^2} + \frac{1}{a^2 + (x + \bar{x}_{-1})^2} \right], \quad (\text{B7})$$

$$\Psi_0^{0,0}(0, 1; x) \sim \frac{1}{3\pi\Delta\nu_D} \left[\frac{x + \bar{x}_1}{a^2 + (x + \bar{x}_1)^2} + \frac{x}{a^2 + x^2} + \frac{x + \bar{x}_{-1}}{a^2 + (x + \bar{x}_{-1})^2} \right], \quad (\text{B8})$$

$$\Psi_0^{0,1}(0, 1; x) \sim \frac{\sqrt{6}}{6\pi\Delta\nu_D} \left[\frac{x + \bar{x}_1}{a^2 + (x + \bar{x}_1)^2} - \frac{x + \bar{x}_{-1}}{a^2 + (x + \bar{x}_{-1})^2} \right], \quad (\text{B9})$$

$$\Psi_0^{0,2}(0, 1; x) \sim \frac{\sqrt{2}}{6\pi\Delta\nu_D} \left[\frac{x + \bar{x}_1}{a^2 + (x + \bar{x}_1)^2} - \frac{2x}{a^2 + x^2} + \frac{x + \bar{x}_{-1}}{a^2 + (x + \bar{x}_{-1})^2} \right]. \quad (\text{B10})$$

Summing the various terms in the square parenthesis, each of the previous profiles can be expressed as a single ratio of polynomials. Taking the leading order in x in the numerator and denominator, one reaches the following limits for their ratios over $\Phi_0^{0,0}(0, 1; x)$,

$$\begin{aligned} \frac{\Phi_0^{0,0}(0, 1; x)}{\Phi_0^{0,0}(0, 1; x)} &= 1, & \lim_{x \rightarrow \infty} \frac{\Phi_0^{0,1}(0, 1; x)}{\Phi_0^{0,0}(0, 1; x)} &\rightarrow 0, & \lim_{x \rightarrow \infty} \frac{\Phi_0^{0,2}(0, 1; x)}{\Phi_0^{0,0}(0, 1; x)} &\rightarrow 0, \\ \lim_{x \rightarrow \infty} \frac{\Psi_0^{0,0}(0, 1; x)}{\Phi_0^{0,0}(0, 1; x)} &\rightarrow \infty, & \lim_{x \rightarrow \infty} \frac{\Psi_0^{0,1}(0, 1; x)}{\Phi_0^{0,0}(0, 1; x)} &\rightarrow \frac{\sqrt{6}}{3} \frac{\nu_L}{a\Delta\nu_D}, & \lim_{x \rightarrow \infty} \frac{\Psi_0^{0,2}(0, 1; x)}{\Phi_0^{0,0}(0, 1; x)} &\rightarrow 0. \end{aligned}$$

Thus, the only off-diagonal element of the propagation matrix that, divided by η_I , does not eventually fall to zero as x increases is ρ_V/η_I . This ratio instead reaches the constant value

$$\lim_{x \rightarrow \infty} \frac{\rho_V(x, \mathbf{\Omega})}{\eta_I(x, \mathbf{\Omega})} \rightarrow \frac{4\pi\nu_L \cos \alpha}{\Gamma}. \quad (\text{B11})$$

One immediate conclusion is that, far enough from the line center, the ρ_V/η_I ratio is independent of the Doppler width of the line and it scales linearly with the magnetic field strength. In the absence of collisions, Γ simply becomes the Einstein coefficient for spontaneous emission $A(\beta_u L_u S J_u \rightarrow \beta_\ell L_\ell S J_\ell)$. Interestingly, the onset of the Hanle effect is likewise determined by the ratio of the Larmor frequency associated to the ambient magnetic field ν_L over the line-broadening parameter Γ . For a two-level atom the efficacy of the Hanle effect is characterized by the parameter $H_u = (2\pi\nu_L g_u)/A(\beta_u L_u S J_u \rightarrow \beta_\ell L_\ell S J_\ell)$, where g_u is the Landé factor of the upper level, and for which the role played by collisions has also been neglected. This illustrates why one should expect the modification of the scattering polarization signatures in the line core (due to the Hanle effect) and in the line wings (produced by magneto-optical effects) to become significant at similar magnetic field strengths. Furthermore, the relation between the magnetic field strength (through the Larmor frequency) and \bar{x}_q , given in Equation (A8), implies that $\nu_L = (\bar{\nu}_{-1} - \bar{\nu}_1)/2$. Thus, the far-wing limit given in Equation (B11) can be directly related to the frequency separation between the centers of gravity of the σ_b and σ_r components as

$$\lim_{x \rightarrow \infty} \frac{\rho_V(x, \mathbf{\Omega})}{\eta_I(x, \mathbf{\Omega})} \rightarrow \frac{2\pi(\bar{\nu}_{-1} - \bar{\nu}_1) \cos \alpha}{\Gamma}. \quad (\text{B12})$$

C. THE TWO-TERM ATOM IN THE INCOMPLETE PASCHEN-BACK REGIME

We can now generalize the results presented in Appendix. B to the case of a two-term atom with arbitrary values of S , L_u , and L_ℓ , accounting for the IPB effect. Taking a reference frame for which the quantization axis is along the magnetic field direction,

the elements of the propagation matrix given in Eqs. (A9) and (A10) can be rewritten as

$$\begin{aligned}\eta_I &= k_M \left[\frac{\sqrt{3}}{3} \sum_q (-1)^{1+q} \begin{pmatrix} 1 & 1 & 0 \\ q & -q & 0 \end{pmatrix} \phi_q(x) + \frac{\sqrt{30}}{12} (3 \cos^2 \alpha - 1) \sum_q (-1)^{1+q} \begin{pmatrix} 1 & 1 & 2 \\ q & -q & 0 \end{pmatrix} \phi_q(x) \right], \\ \eta_V &= k_M \frac{\sqrt{6}}{2} \cos \alpha \sum_q (-1)^{1+q} \begin{pmatrix} 1 & 1 & 1 \\ q & -q & 0 \end{pmatrix} \phi_q(x), & \eta_Q &= k_M \frac{\sqrt{30}}{4} \sin^2 \alpha \sum_q (-1)^{1+q} \begin{pmatrix} 1 & 1 & 2 \\ q & -q & 0 \end{pmatrix} \phi_q(x), \\ \rho_V &= k_M \frac{\sqrt{6}}{2} \cos \alpha \sum_q (-1)^{1+q} \begin{pmatrix} 1 & 1 & 1 \\ q & -q & 0 \end{pmatrix} \psi_q(x), & \rho_Q &= k_M \frac{\sqrt{30}}{4} \sin^2 \alpha \sum_q (-1)^{1+q} \begin{pmatrix} 1 & 1 & 2 \\ q & -q & 0 \end{pmatrix} \psi_q(x).\end{aligned}\quad (C1)$$

Considering a frequency far enough from the line center that the asymptotic expansion in Equation (A13) can be applied to the absorption profiles, the ϕ_q and ψ_q profiles become

$$\phi_q(x) = \sum_{r=1}^N \frac{a}{\pi \Delta \nu_D} S_q^r \frac{1}{a^2 + (x + x_r)^2}, \quad \psi_q(x) = \sum_{r=1}^N \frac{1}{\pi \Delta \nu_D} S_q^r \frac{x + x_r}{a^2 + (x + x_r)^2}.$$

The label r stands for the set of quantum numbers (j_u, M_u, j_ℓ, M_ℓ) that correspond to the transition between states $|\beta_u L_u S j_u M_u\rangle$ and $|\beta_\ell L_\ell S j_\ell M_\ell\rangle$ and N is the total number of distinct transitions between the two terms. As in the derivation presented in the previous section, the ratios of polynomials appearing in the profiles can be summed into a single ratio. In order to obtain the expressions for the elements of the propagation matrix presented below, which are valid where $x \gg 1$, we have used the identities

$$\sum_{r=1}^N S_q^r = 1, \quad \sum_{r=1}^N S_q^r x_r \equiv \bar{x}_q = -q (v_L / \Delta \nu_D), \quad \sum_{s \neq r} x_s = -x_r,$$

We recall that the last equality in the second identity holds in the IPB effect regime, while the spectral shifts \bar{x}_q are instead overestimated when the LZS approximation is made. We have also used the following useful relations for the Racah algebra $3j$ symbols:

$$\begin{aligned}\sum_q (-1)^{1+q} \begin{pmatrix} 1 & 1 & 0 \\ q & -q & 0 \end{pmatrix} &= \sqrt{3}, & \sum_q (-1)^{1+q} \begin{pmatrix} 1 & 1 & 1 \\ q & -q & 0 \end{pmatrix} &= 0, & \sum_q (-1)^{1+q} \begin{pmatrix} 1 & 1 & 2 \\ q & -q & 0 \end{pmatrix} &= 0, \\ \sum_q (-1)^{1+q} q \begin{pmatrix} 1 & 1 & 0 \\ q & -q & 0 \end{pmatrix} &= 0, & \sum_q (-1)^{1+q} q \begin{pmatrix} 1 & 1 & 1 \\ q & -q & 0 \end{pmatrix} &= \frac{\sqrt{6}}{3}, & \sum_q (-1)^{1+q} q \begin{pmatrix} 1 & 1 & 2 \\ q & -q & 0 \end{pmatrix} &= 0.\end{aligned}$$

Taking only the leading orders in x for both the numerator and denominator, after some tedious algebra one reaches the following expressions for the elements of the propagation matrix

$$\eta_I(x, \Omega) \approx k_M \frac{1}{\pi \Delta \nu_D} \frac{a}{x^2}, \quad (C2a)$$

$$\eta_V(x, \Omega) \approx k_M \frac{2a}{\pi \Delta \nu_D} \frac{1}{x^3} \frac{v_L}{\Delta \nu_D} \cos \alpha, \quad \eta_Q(x, \Omega) \approx k_M \frac{\sqrt{30}}{4\pi \Delta \nu_D} \frac{a}{x^4} \sin^2 \alpha \sum_q (-1)^{1+q} \begin{pmatrix} 1 & 1 & 2 \\ q & -q & 0 \end{pmatrix} v_q, \quad (C2b)$$

$$\rho_V(x, \Omega) \approx k_M \frac{1}{\pi \Delta \nu_D} \frac{1}{x^2} \frac{v_L}{\Delta \nu_D} \cos \alpha, \quad \rho_Q(x, \Omega) \approx k_M \frac{\sqrt{30}}{4\pi \Delta \nu_D} \frac{1}{x^3} \sin^2 \alpha \sum_q (-1)^{1+q} \begin{pmatrix} 1 & 1 & 2 \\ q & -q & 0 \end{pmatrix} w_q, \quad (C2c)$$

where

$$v_q = \sum_{r=1}^N S_q^r \left(\sum_{s \neq r} x_s^2 + 4 \sum_{s \neq r} x_s \sum_{\substack{t > s \\ t \neq r}} x_t \right), \quad w_q = \sum_{r=1}^N S_q^r \left(\sum_{s \neq r} x_s^2 + 4 \sum_{s \neq r} x_s \sum_{\substack{t > s \\ t \neq r}} x_t - 2 x_r^2 \right). \quad (C3)$$

It is immediate to realize that, also for a two-term atom with arbitrary values of L_u, L_ℓ , and S , the only coefficient in the propagation matrix whose ratio over η_I does not fall to zero when $x \rightarrow \infty$ is ρ_V . Moreover, the expressions relating such ratio to the Larmor frequency and to the spectral distance between the centers of gravity of the σ_b and σ_r components are also recovered exactly as given in Eqs. (B11) and (B12), respectively. It should be emphasized that this proof is based on the relation $\bar{x}_q = -q v_L / \Delta \nu_D$, which is strictly valid in the IPB effect regime. In contrast, making the LZS approximation may introduce significant errors in the determination of the far-wing value of the ρ_V / η_I relation, even in the presence of relatively weak magnetic fields.

REFERENCES

- Belluzzi, L., Trujillo Bueno, J., & Štěpán, J. 2012, *ApJ*, 755, L2
- Condon, E. U., & Shortley, G. H. 1935, *The Theory of Atomic Spectra* (Cambridge: Cambridge University Press)
- del Pino Alemán, T., Casini, R., & Manso Sainz, R. 2016, *ApJ*, 830, L24
- Fontenla, J. M., Avrett, E. H., & Loeser, R. 1993, *ApJ*, 406, 319
- Kano, R., Trujillo Bueno, J., Winebarger, A., et al. 2017, *ApJ*, 839, L10
- Landi Degl'Innocenti, E. 1983, *Sol. Phys.*, 85, 3
- . 2014, *Atomic Spectroscopy and Radiative Processes* (Verlag Mailand: Springer)
- Landi Degl'Innocenti, E., Bommier, V., & Sahal-Brechot, S. 1991, *A&A*, 244, 391
- Landi Degl'Innocenti, E., & Landolfi, M. 2004, *Polarization in Spectral Lines* (Dordrecht: Kluwer Academic Publishers)
- Przybilla, N., & Butler, K. 2004, *ApJ*, 609, 1181
- Socas-Navarro, H., Trujillo Bueno, J., & Landi Degl'Innocenti, E. 2004, *ApJ*, 612, 1175
- Trujillo Bueno, J., Štěpán, J., & Casini, R. 2011, *ApJ*, 738, L11
- Trujillo Bueno, J., Štěpán, J., Belluzzi, L., et al. 2018, *ApJ*, 866, L15
- Štěpán, J., Trujillo Bueno, J., Leenaarts, J., & Carlsson, M. 2015, *ApJ*, 803, 65